J. Fluid Mech. (1975), *vol.* 72, *part* 3, *pp.* 481–498
Printed in Great Britain

Turbulent and laminar pipe flow distorted by magnetic forces

By A. J. YULE

Department of Engineering, University of Warwick, Coventry, England†

(Received 18 October 1973 and in revised form 2 July 1975)

A flow of an electrolyte in a seventy-diameter length of round pipe is subjected to a two-dimensional electric current and magnetic field which give a controllable streamwise electromagnetic body force. As the body-force distribution is axisymmetric and the effects of induced currents are negligible the fully developed pipe flow is axisymmetric and longitudinally homogeneous, but it can have severely distorted mean velocity and turbulence profiles. Measurements of the mean velocity and turbulence intensity are presented for different levels of distortion and the results are discussed with reference to classical turbulence theories. The inadequacy of these theories is thus demonstrated. The extra degree of freedom provided by the body force combines with the relative simplicity of the fully developed flow to give a useful tool for investigating the nature of shear-flow turbulence and for studying the assumptions involved in analytical approaches. The technique also produces distorted laminar pipe flows with inflexion-point velocity profiles, which are of interest in stability studies.

1. Introduction

Numerous experiments have attempted to throw light on the structure of turbulence by applying distortions to fully developed flows, e.g. applying pressure gradients to wake flow. The interpretation of measurements in such flows is often hampered by their complexity and it is likely that advances in the physical understanding of turbulence must first involve a more detailed knowledge of fully developed and self-preserving turbulent flows. Fully developed pipe flow has the advantages of simplified equations of motion and a known shear-stress distribution. The main objective of this investigation was to establish the feasibility of severely distorting pipe flow but to retain the above advantages. It is shown below how electromagnetic body forces were used to distort the flow while true MHD effects, with their unwanted complications, were kept negligible.

The present flows have close similarities to some practical flows. Axisymmetric electromagnetic induction pumps with a.c. travelling fields exist which produce mean streamwise body forces proportional to the square of the distance from the pipe centre as in the present experiments. Similar travelling-field configurations are in wide use for stirring metallurgical furnaces but in both applications there is

† Present address: Department of Chemical Engineering and Fuel Technology, University of Sheffield, England.

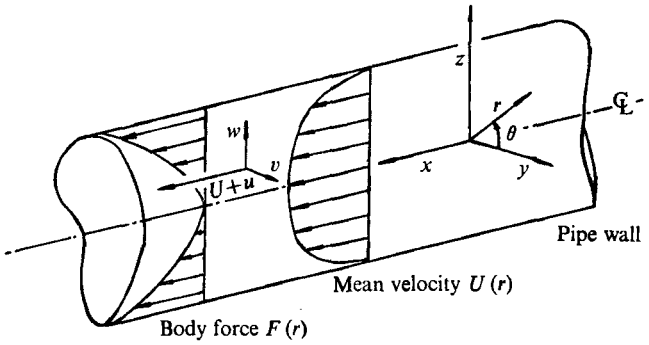

FIGURE 1. Notation for distorted pipe flow.

backflow, which does not occur in the present experiment. Distorted fully developed flows occur in vertically mounted pipes with heated walls; however the applied body force is not directly controllable in this case. Hall & Jackson (1969) studied turbulent flows of this type and Scheele & Greene (1966) described analytical solutions for laminar flows.

2. Equations of motion

2.1. *Body-force distribution*

The distribution of an extra streamwise body force which is compatible with a distorted, axisymmetric, fully developed pipe flow must itself be axisymmetric and independent of the distance x along the pipe (see figure 1 for the notation). Any continuous function $F(\eta)$ can be used, where F is the applied body force per unit fluid volume and $\eta = r/R$, where r is the distance from the pipe axis and R is the pipe radius. The equation of motion is

$$F - r^{-1}\rho\,\partial(\overline{uv}r)/\partial r - dP/dx + \nu\rho r^{-1}\,\partial[r(\partial U/\partial r)]/\partial r = 0, \tag{1}$$

where U is the local mean velocity, u and v are the fluctuating components of the velocity, ν is the kinematic viscosity, P is the wall static pressure and ρ is the density of the fluid. The x axis is defined such that $U \to 0$ through positive values as $r \to R$.

The similarity forms for fully developed flow are $U = u_\tau f(\eta)$ and $\overline{uv} = u_\tau^2 g(\eta)$, where u_τ is the friction velocity, defined by $u_\tau = [-\nu\,\partial U/\partial r]^{\frac{1}{2}}_{r=R}$. Equation (1) becomes

$$(R/\rho u_\tau^2)F(\eta) - \eta^{-1}d(g\eta)/d\eta - (R/\rho u_\tau^2)dP/dx + R_\tau^{-1}\eta^{-1}d(f'\eta)/d\eta = 0, \tag{2}$$

where $R_\tau = u_\tau R/\nu$. The friction velocity and pressure gradient are independent of x, as in normal pipe flow.

2.2. *Magnetic and electric current fields*

The experimental requirement was a means of applying an axisymmetric streamwise body-force distribution to a long length of pipe flow without otherwise interfering with the flow. This was achieved by applying suitably designed electric

current and magnetic fields. Consider a conducting fluid in a pipe with applied fields **j** and **B**, where **j** is the current density vector and **B** is the magnetic flux density vector. As is discussed later the fluid conductivity, velocities and field strengths are selected to give negligible induced currents. To satisfy the requirements on F the **j** and **B** fields are independent of x and have no components in the x direction since the aim is to have the $\mathbf{j} \times \mathbf{B}$ force in the x direction. The fields are written in terms of complex variables $\alpha(Z)$ and $\beta(Z)$, where Z is the complex number $y+iz$ and y and z are Cartesian co-ordinates in the transverse plane:

$$B_y - iB_z = \alpha'(Z), \quad j_y - ij_z = \beta'(Z), \tag{3), (4}$$

where suffixes denote field components and a prime denotes differentiation with respect to Z. The resulting body force is in the x direction with a magnitude, using mks units,

$$F = j_y B_z - j_z B_y. \tag{5}$$

Equations (3)–(5) give

$$F = -\mathscr{I}(\alpha'\beta'^*) = -(\alpha'\beta'^* - \alpha'^*\beta')/2i, \tag{6}$$

where the asterisks denote complex conjugates. All possible body-force profiles may be obtained by choosing suitable expressions for α and β. In the present case α and β are constrained as F is axisymmetric and thus $F = F(ZZ^*)$, or $Z^*\partial F/\partial Z^* = Z\,\partial F/\partial Z$. With this condition (6) gives the permitted forms of α' and β' as

$$\alpha' = k_1(Z^m + \lambda Z^n), \quad \beta' = k_2 i(Z^{m*} - \lambda Z^{n*}) \tag{7), (8}$$

and thus

$$F = k_1 k_2 (r^{2m} - \lambda\lambda^* r^{2n}), \tag{9}$$

where k_1 and k_2 are real coefficients which are proportional to the strengths of the applied magnetic and current fields respectively and m, n and λ are independent parameters. A further constraint on the applied fields is imposed by practical difficulties in constructing the apparatus. The complexity of the fields increases with increasing m, n and λ, and the simplest case, with $m = 1$ and $\lambda = 0$, was selected. Also, the body-force distribution for this case produces appreciable distortion over a greater width of the pipe than would be affected with higher values of the variables. Equation (9) becomes

$$F = k_1 k_2 r^2, \tag{10}$$

and the field strengths are

$$B = k_1 r, \quad j = k_2 r. \tag{11}$$

As is shown in figure 2, the field lines are orthogonal hyperbolas, which represent four magnetic poles and four current sources/sinks which are $\frac{1}{4}\pi$ out of phase in space.

2.3. *Equations of motion with parabolic body force*

The body force in (10) is written in a dimensionless form such that

$$RF/\rho u_\tau^2 = 4K\eta^2, \tag{12}$$

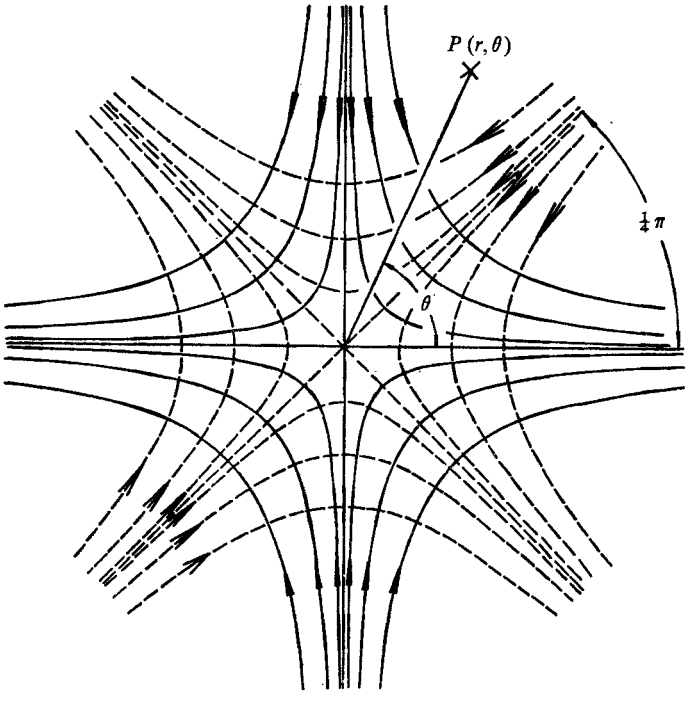

FIGURE 2. Field lines required for an axisymmetric body-force distribution $F \propto r^2$. ——, magnetic field; – – –, current field.

where K is the dimensionless group $k_1 k_2 R^3/4\rho u_\tau^2$, which represents the ratio of applied body forces to shear forces in the pipe. Substituting for F in (2) gives, for fully developed flow,

$$4K\eta^2 - \eta^{-1} d(g\eta)/d\eta - (R/\rho u_\tau^2)\, dP/dx + R_\tau^{-1} \eta^{-1} d(f'\eta)/d\eta = 0. \tag{13}$$

The total shear stress is

$$\tau = \overline{uv} - \nu\, \partial U/\partial r. \tag{14}$$

Integrating (13) gives

$$\tau/u_\tau^2 = g - R_\tau^{-1} f' = K\eta^3 - \tfrac{1}{2}\eta (R/\rho u_\tau^2)\, dP/dx \tag{15}$$

and evaluating this at the pipe wall yields $(R/\rho u_\tau^2)\, dP/dx = 2(K-1)$, or

$$u_\tau^2 = (R/2\rho)\, (\tfrac{1}{2} k_1 k_2 R^2 - dP/dx). \tag{16}$$

This is the momentum conservation equation for a complete cross-section of the pipe. When $K = 0$ there are no applied forces and the normal balance between the pressure gradient and the wall shear stress is obtained. When $K = 1$ the applied body forces balance the wall shear stress and there is no pressure gradient in the pipe.

Equation (16) is used to eliminate dP/dx from (15) to give the momentum equation in the form

$$\tau/u_\tau^2 = g - R_\tau^{-1} f' = K\eta(\eta^2 - 1) + \eta. \tag{17}$$

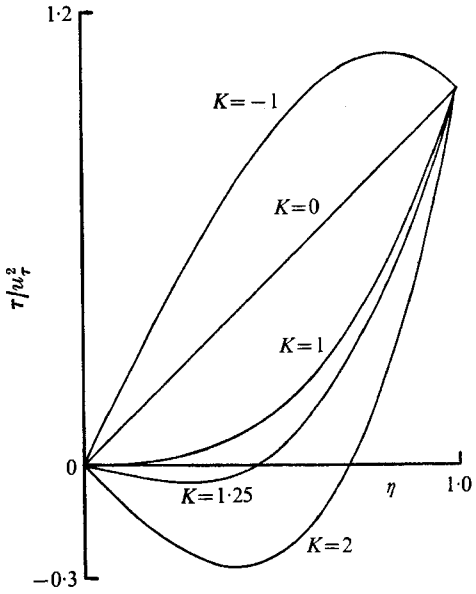

FIGURE 3. Calculated distributions of the total shear stress across turbulent or laminar pipe flows with different levels of applied body force.

The body force thus gives cubic contributions to the total shear stress, which is known in the pipe when K is known. Shear-stress distributions calculated for different values of K are shown in figure 3.

The turbulent energy equation is not changed by the body force, so that

$$\overline{uv}\,\partial U/\partial r + r^{-1}\partial(\tfrac{1}{2}\overline{q^2 vr} + \rho^{-1}\overline{pv}r)/\partial r + \epsilon = 0, \tag{18}$$

where q^2 is the sum of the turbulence intensity components, p is the fluctuating pressure and ϵ is the viscous dissipation per unit fluid volume.

2.4. *Laminar flow solution*

For fully developed laminar flow $g = 0$ and (17) gives

$$f = U/u_\tau = R_\tau\{\tfrac{1}{2}(1-\eta^2) - \tfrac{1}{4}K(1-\eta^2)^2\}, \tag{19}$$

or, in terms of the centre-line velocity U_1,

$$U/U_1 = (1-\tfrac{1}{2}K)^{-1}\{(1-\eta^2) - \tfrac{1}{2}K(1-\eta^2)^2\}. \tag{20}$$

Figure 4 gives some of the calculated velocity profiles for different values of K. A positive value of K implies electromagnetic forces which are acting in the same direction as the flow near the pipe wall. For laminar flow with $K > 1$ there are twin velocity peaks and for $K > 2$ there is a recirculation region near the centre of the pipe. For increasingly negative values of K there is a tendency towards a jet-like velocity profile until $K = -\infty$, when there is no wall shear stress. For all values of K outside the range $-\frac{1}{2} \leqslant K \leqslant 1$ there is an inflexion point at

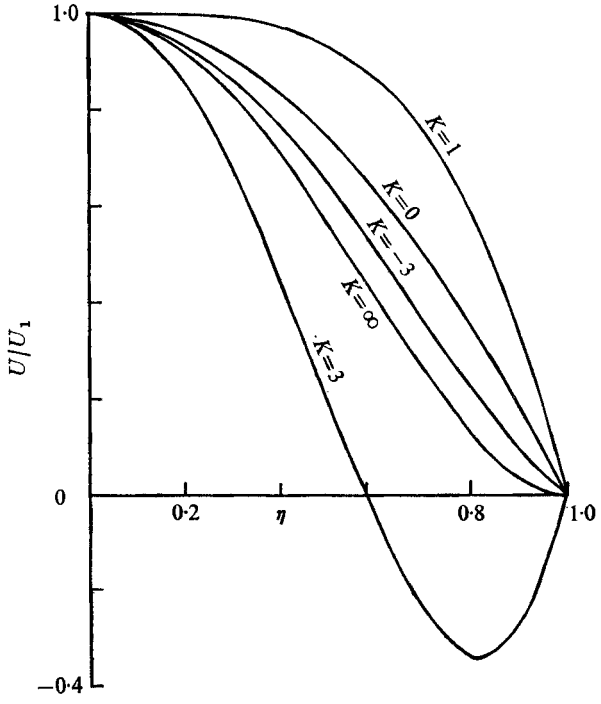

FIGURE 4. Calculated velocity profiles for distorted laminar pipe flows.

$\eta = \{(K-1)/3K\}^{\frac{1}{2}}$, which makes these flows of particular interest in stability studies. The application of turbulence theories to the distorted turbulent flow is discussed in §5.

3. Experiment

3.1. *Production of fields*

A pipe diameter of around 50 mm was considered a reasonable size in which to make measurements but small enough to match the available facilities. In order that the pipe flows had a good chance of becoming fully developed it was decided that they should be subjected to the body force for at least 50 pipe diameters. A cross-section of the magnet and pipe is shown in figure 5. The four-pole mild-steel magnet was 3·05 m long and the distance between opposite pole faces was 58·5 mm. The upper and lower poles each had 24 turns of water-cooled copper coils and the pole faces were machined to the required hyperbolic shape. The magnet was powered by accumulators giving up to 200 A at 24 V. The field inside the magnet was measured by a small Hall probe and was found to agree with (11) to within 1%. The maximum flux density obtainable was 0·5 tesla, measured at the pole faces.

The production of the required current field in the conducting fluid in the pipe was a basic design problem owing to the need for a continuously varying voltage at the pipe wall. The use of longitudinal strip electrodes at the pipe wall was rejected because of the lack of perfect axisymmetry which would result. The final

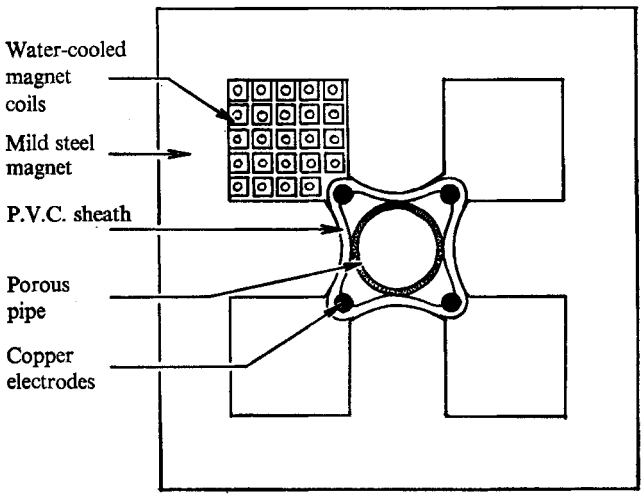

FIGURE 5. Cross-section of magnet and test section.

configuration is shown in figure 5. The pipe was constructed from Celloton, a porous ceramic material, and had an internal diameter of 43·2 mm and a wall thickness of 2·5 mm. The working fluid, copper sulphate solution, was absorbed by the pipe wall, thus enabling currents to pass through the wall. Copper sulphate solution was chosen as it gave off no gases due to electrolysis when used with the copper electrodes. The four electrodes were 9·5 mm diameter copper rods which were supplied by accumulators. The assembly was enclosed and held together by an outer PVC sheath which was completely filled with copper sulphate solution and was positively located at the centre of the magnet by the pole faces. The sheath, electrodes and pipe assembly extended the full length of the magnet so that the pipe flow was subjected to the body force for 70 pipe diameters.

As the conductivity of the test pipe when soaked in the conducting fluid was a constant fraction of the fluid conductivity (about $\frac{1}{4}$) changes in the conductivity of the test fluid with temperature or concentration had no effect on the geometry of the current field. If the conductivity of the soaked pipe had been the same as that of the conducting fluid the sheath wall shape would have followed the hyperbolic current field lines. The differing conductivities required an analytical solution for the sheath wall shape, obtained by solving the boundary-value problem with the solution properties specified at the pipe wall by the required current distribution. The current field in the pipe wall and thus outside the pipe was derived. The current field line which just touched the outer pipe wall gave the sheath wall shape. A test rig consisting of a 0·1 m length of the sheath/electrodes/pipe assembly was made. The current inside the pipe agreed with (11) to within 2 % when electrode potentials of up to 30 V were used. The current and magnetic fields thus gave an axisymmetric body force in the pipe which agreed with (10) to within 5 % at worst.

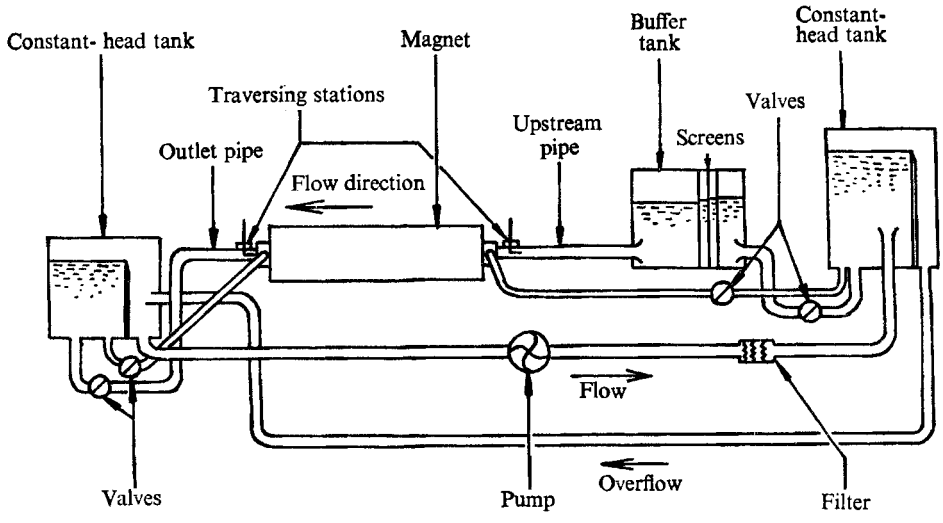

FIGURE 6. Schematic diagram of flow circuit.

3.2. *Flow circuit*

As is shown in figure 6, the copper sulphate solution was passed through the test section via a closed circuit incorporating upstream and downstream constant-head tanks, filters and a buffer tank with screens. The 45 diameters length of Perspex entry pipe gave a normal fully developed flow at the entry to the test section. A secondary flow system passed test fluid through the spaces between the test pipe and the outer sheath, thus cooling the electrodes and removing copper debris deposited at the negative electrodes by electrolysis.

The linear voltage drops along the electrodes (due to their resistances) were countered by feeding the positive and negative electrodes from opposite ends, thus ensuring a constant potential difference between adjacent electrodes.

The pressure difference between the inside and the outside of the test pipe was always adjusted to be less than 10 mm of water so that cross-flow velocities through the pipe wall were negligible. Preliminary experiments indicated that these velocities were always at least three orders of magnitude less than the maximum velocity in the pipe.

The inlet and outlet pipes and the test pipe were set up to within 50 μm of the centre-line of the magnet by using an optical micrometer telescope.

3.3. *Probes and instrumentation*

It was not necessary to know the exact value of the conductivity of the test fluid as knowledge of the applied current and magnetic fields (obtained from a calibration of the magnet) gave the strength and distribution of the body force directly. Static-pressure tappings were drilled at intervals along the walls of the inlet and outlet pipes.

DISA type 55 F06 and 55 F09 nickel-coated fibre hot films were used. The thickness 2 μm of the quartz insulating layer on these films was not sufficient to

cope with the potential differences of up to 24 V which could exist across the pipe diameter in the experiments. This difficulty was overcome by de-earthing the probe and electronic equipment and 'floating' them at the local fluid potential by removing the insulation from one of the prongs of the probe. Traversing stations were built into the inlet and outlet pipes so that probes could be traversed across the beginning of the test pipe and also inside the last 50 mm of the test pipe inside the magnet. Traverses were driven by a stepper motor at speeds of approximately 1 mm/s. A Thermosystems 1010 constant-temperature anemometer was used and the output was linearized in the range of velocities used by a DISA 55D10 linearizer. The probes were calibrated in the range $0{\cdot}05\,\mathrm{m/s} < U < 1\,\mathrm{m/s}$ by using a towing tank and the calibrations were monitored by a Pitot tube in the inlet pipe. The mean and r.m.s. voltage outputs of the linearizer were recorded by x, y plotters synchronized with the stepper motor. The r.m.s. signal, representing $(\overline{u^2})^{\frac{1}{2}}$, was obtained via a Hewlett Packard H12-3400A r.m.s. voltmeter which had a lower frequency limit of 2 Hz.

Some mean velocity measurements were also made with a multiple Pitot comb which could be positioned inside the porous pipe and rotated to measure the velocity distribution across any pipe diameter.

3.4. *Restrictions on the magnitude of the applied body force*

The objective in the design of the experiment was to produce an extra, directly controllable $\mathbf{j} \times \mathbf{B}$ force in the pipe flow without any appreciable MHD effects. Such effects would entail induced currents in the flow leading to such unwanted phenomena as the direct suppression of turbulence and loss of axisymmetry. The relative importance of MHD effects can be deduced from the values of the dimensionless groups associated with the flow, namely the magnetic force coefficient $S = \sigma B^2 R/\rho U_1$ and the Hartmann number $H = BR(\sigma/\rho\nu)$, where σ is the fluid conductivity. The magnetic force coefficient, as discussed by Shercliff (1965, p. 86), indicates the relative importance of magnetic (i.e. MHD) forces and inertia forces when the magnetic Reynolds number is small. The magnetic Reynolds number $\mu\sigma U_1 R$, where μ is the permeability of free space, is of the order 10^{-6} in the present experiments and is thus negligible. The Hartmann number is a measure of the relative importance of magnetic and viscous forces. The Reynolds number $R_1 = U_1 R/\nu$ is of the order 10^4 and as $S = H^2 R_1^{-1}$ the value of S is always much less than unity when H is small. The Hartmann number is thus the critical parameter with regard to MHD effects in the distorted pipe flow. In the experiments $\sigma = 10\,\mathrm{mho/m}$ and $\nu = 10^{-6}\,\mathrm{m^2/s}$, which gives $H \approx 2B$, so that magnetic fields in the test pipe of the order of 0·1 tesla should be acceptable. When traverses of the flow were made with an applied magnetic field but no current field no measurable distortions of the normal pipe-flow velocity profile were found for peak values of B less than 0·2 tesla.

Reducing the test fluid's conductivity allows higher magnetic field strengths to be used but it does not necessarily permit the use of higher electromagnetic body forces. This is because the maximum applied current was limited by the requirement of low heating rates of the test fluid so that the flow itself and the

hot-film calibrations were not significantly changed. In fact the restrictions on the heating rate and the Hartmann number imply that there is no advantage to be gained by varying the fluid conductivity, i.e. lowering the value of σ enables higher magnetic field strengths to be used but smaller values of the current field would be necessary to keep heating effects negligible. The maximum usable current was found by checking the calibration of a hot-film probe downstream of the test section and also the measured mean velocity profile with and without an applied current field. No detectable changes in the mean velocity measurements (implying changes of less than 5 % in the actual velocities) were found for maximum electrode currents less than 150 A when U_1 was 0·5 m/s. The measured temperature rise at the end of the test section was then 2 °C.

In practice the above considerations restricted the usable range of the body-force coefficient to approximately $-1{\cdot}5 < K < +1{\cdot}5$ (for fully turbulent flow with $R_1 = 5000$).

4. Experimental results

4.1. *Preliminary experiments*

The Pitot comb was used to check that the distorted pipe flows were axisymmetric and fully developed at the end of the magnet. Mean velocity profiles were measured across different diameters and at several longitudinal positions in the last 0·5 m of the test pipe. These profiles were axisymmetric and similar to within 5 %, which was within the accuracy of the Pitot-tube/manometer combination. It was concluded that the distorted pipe flows were axisymmetric and fully developed at the end of the test pipe (where the hot-film measurements were subsequently made). The mean velocity profiles for $K = 0$ were in good agreement with Laufer's (1955) and other published results. Accurate measurements with the Pitot tubes required $R_1 > 10^4$, and K was then restricted to the range $-0{\cdot}3 < K < +0{\cdot}3$ approximately. The use of the hot films removed this restriction and allowed lower velocities with higher levels of distortion to be used.

4.2. *Results of hot-film measurements*

For fully turbulent pipe flows it was necessary for R_1 to be greater than 2×10^3 approximately, which required $R_\tau > 10^2$ for both normal and distorted flows. Figure 7 shows typical x, y recorder plots of the anemometer d.c. and r.m.s. outputs for traverses across the pipe with positive values of K. The twin peaks of the distorted fully developed flow are evident. Traverses were made with a large number of distorted flows and excellent repeatability was found for both the mean and r.m.s. measurements. Figure 8 gives measured mean velocity profiles for normal and distorted pipe flows with approximately the same values of the wall shear stress, so that $R_\tau \approx 200$ or $R_1 \approx 5000$. The value of the shear velocity u_τ, which was required for normalizing the measurements and also for deriving the values of R_τ and K, was calculated using (16) and the known values of k_1 and k_2 with the measured wall pressure gradient. The mean velocity measurements

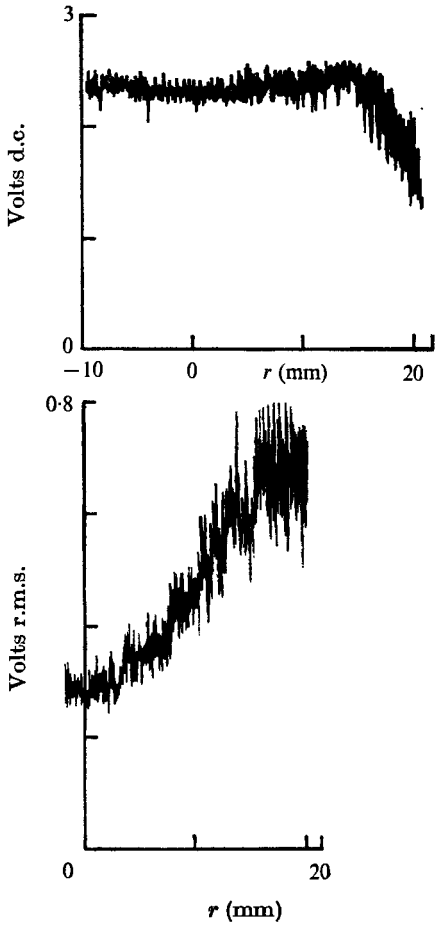

FIGURE 7. Typical x, y recorder plots representing mean velocity and turbulence intensity for a traverse across a distorted flow.

agree with previous results for undistorted flows and also with the Pitot-tube measurements.

Normalized turbulence intensity measurements are shown in figure 9 for normal pipe flow and for positive and negative values of K. The turbulence intensities are in general about 10 % below those of Laufer (1955) for $K = 0$. This discrepancy is thought to be due to the loss of the very low frequency components $2\pi Rn/U_1 < 0{\cdot}2$ caused by the instrumentation.

Some traverses were made with laminar pipe flows with $R_1 \approx 100$. At this low Reynolds number natural convection was a noticeable effect and there was a lack of symmetry in the flows. Furthermore calibration of the hot films at these low velocities was difficult and considerable drift occurred in the calibrations. However, the results of traverses with $K = 0$ and $K \approx 2$ are given in figure 10 for their qualitative interest. The distortion of the normal parabolic velocity distribution into a twin-peaked distribution with inflexion points may be seen.

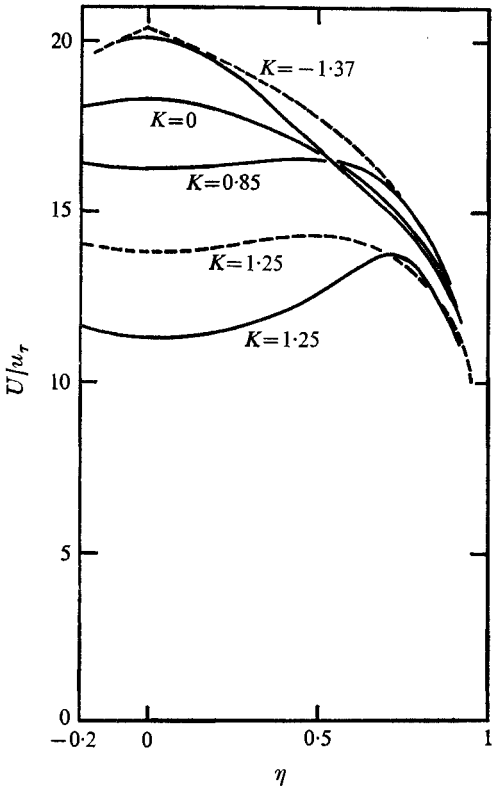

FIGURE 8. Mean velocity distributions across distorted pipe flows. ——, measured; – – –, mixing-length solution.

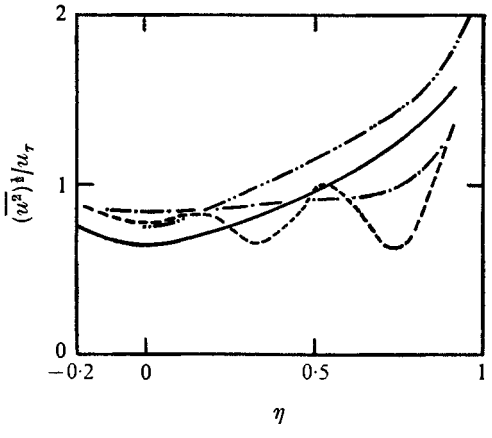

FIGURE 9. Measured turbulence intensity distributions across distorted pipe flows. ——, $K = 0$; – – –, $K = 1{\cdot}25$; —·—, $K = -0{\cdot}89$; —··—, Laufer (1955).

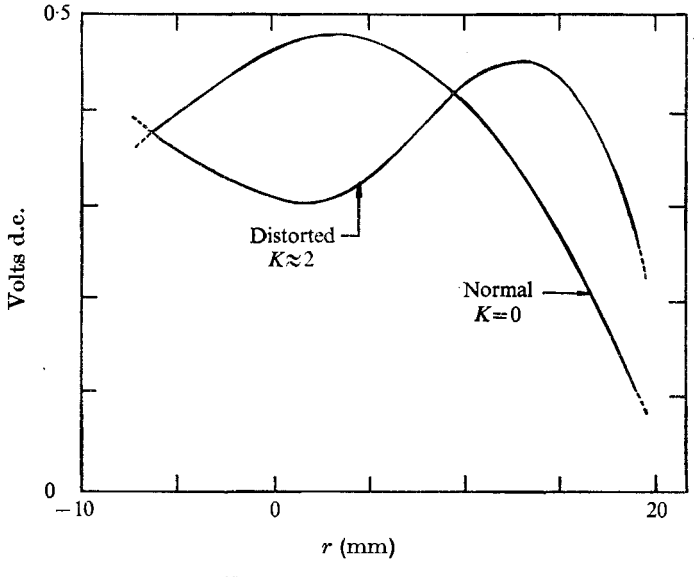

FIGURE 10. Hot-film measurements with laminar pipe flow.

5. Discussion

The measurements demonstrate that distorted, axisymmetric, fully developed turbulent pipe flows were achieved with good experimental accuracy. It can be seen from figure 8 that turbulent flows with the parabolic body force in the flow direction tended to have twin-peaked velocity profiles, e.g. when $K = 1{\cdot}25$. Velocity profiles with sharper central peaks were produced when the extra body force was acting against the flow, e.g. $K = -1{\cdot}37$. In the range of distorted turbulent flows which was possible with the apparatus the most distorted mean velocity distribution had twin peaks which were more than 20 % higher than the centreline velocity. The position of the peak for favourable body forces moved towards the wall with increasing K. It was particularly noticeable that the favourable body forces produced comparatively more distortion of the mean velocity profile than adverse forces of the same magnitude.

It was not possible to produce turbulent pipe flows with backflow or jet-like velocity profiles with zero wall shear stress as the magnetic and current fields required would have been strong enough to produce significant MHD or heating effects. It is thought that such distorted flows could be achieved without these effects by using pipe diameters several times larger than that used here. The relative sizes of the hot films and the pipe did not allow measurements to be made in the wall region of the flow. However, the other measurements suggest that this region may not have altered significantly in the range of K used, at least compared with the distortions found in the central 'fully turbulent' region $0 < \eta < 0{\cdot}9$ approximately. The single hot films did not permit a detailed investigation of the modified turbulence structure in the time available. It is considered that the use of laser anemometry would provide considerably more data on this type of flow. Mounting the test pipe vertically would allow the effects of heating to be known and axisymmetric when they are unavoidable (with laminar flows or very high distortions) and it would also remove the problem of avoiding air bubbles when filling the apparatus. In spite of the above restrictions the present measurements allow some general observations to be made regarding the distorted flows and some interesting aspects of classical turbulence hypotheses can be seen.

The turbulence intensity distributions in figure 9 indicate that the turbulence structure changes significantly with the application of the body force. For high negative values of K there is a flatter distribution of $(\overline{u^2})^{\frac{1}{2}}/u_\tau$ across the pipe, which can be reconciled qualitatively with the relatively higher values of the velocity gradient and shear stress which exist away from the pipe wall; see figure 3 with $K = -1$. These higher values imply that the turbulent energy production $-\overline{uv}\,\partial U/\partial r$ is significant over a greater width of the flow and does not have the high concentration near the wall found in normal pipe flow. For high positive K, e.g. $K = 1{\cdot}25$ in figure 9, extra troughs occur in the intensity distribution away from the centre of the pipe. The outer trough is near the peak of the distorted mean velocity distribution, which is reasonable as this is a position of zero turbulent energy production. It is interesting to note that the peaks of the measured mean velocity distributions which occurred away from the centre of the pipe for $K > 1$ were always nearer to the pipe wall than the zero crossing of

the calculated shear-stress distribution. For example, comparing the $K = 1{\cdot}25$ distributions in figures 3 and 8, the $\overline{uv}$ zero crossing is at $\eta = 0{\cdot}45$ and the U peak is at $\eta = 0{\cdot}73$. This means that there are two distinct positions of zero turbulent energy production, where $dU/dr = 0$ and where $\overline{uv} = 0$, and between these positions the production term in the turbulent energy balance is negative. A similar phenomenon occurs in certain asymmetric channel flows and it has been the subject of some interest in the past, e.g. Brodkey *et al.* (1973). It is unlikely that any remarkable changes occur in the turbulence structure when regions of negative energy production exist and it is probable that the phenomenon is primarily of interest in demonstrating some of the drawbacks of conventional turbulence theories.

The very clear lack of coincidence in the dU/dr and $\overline{uv}$ zero-crossing positions is a good demonstration of the unsuitability of simple mixing-length or eddy-viscosity assumptions. To show this solutions for the distorted pipe flows obtained with a mixing-length assumption are included in figure 8. It was assumed that $\overline{uv} = -L^2(dU/dr)\,|dU/dr|$, where, following Schlichting (1968, p. 569), $L/R = 0{\cdot}4(1-\eta)\eta^{\frac{1}{2}}$. Equation (17) was solved numerically and matched with the laminar wall solution at $yu_\tau/\nu = 11{\cdot}7$, where y is the perpendicular distance from the pipe wall. The calculated and measured mean velocity profiles agree well for $K = 0$ (this is the log law distribution) but for all of the distorted flows the mixing-length solution significantly underestimates the measured degree of distortion of the profile. The use of more sophisticated forms for L/R and matching in the wall region will not reduce this discrepancy. Solutions using an eddy-viscosity assumption gave even poorer agreement. The basic problem with such methods and also with more advanced energy-equation methods of flow prediction is that the Reynolds averaged equations cannot provide any information on the basic physical mechanisms in the flow. For example observation of oscilloscope traces showed pronounced bursting or spikes in the u signal at a position just on the centre-line side of the outer $(\overline{u^2})^{\frac{1}{2}}/u_\tau$ trough found with positive K. These bursts invite comparison with the wall bursts which have been studied in normal pipe and boundary-layer flows.

It is well known that the mixing-length assumption may be equivalent to assuming an equilibrium structure for the turbulence with the energy production and dissipation terms balancing each other. Thus the present results may indicate the significance of the other terms in the energy equation. In the case of fully developed pipe flows there is no advection of turbulent energy, so that since $\overline{uv}$ is known and ϵ can be estimated an important feature of the present experiment is the information which can be obtained on the diffusion term in the turbulent energy equation (18), as will be discussed below. Some observations on the frequently used assumption of an invariant distribution of the shear coefficient $a_1 = \overline{uv}/\overline{q^2}$ will first be made.

The present experiments have measured $\overline{u^2}$ only but it is reasonable to assume that if $a_1(\eta)$ is independent of the distortion then $\overline{uv}/\overline{u^2}$ will also vary little with K. Examination of the results of Laufer (1955) and Lawn (1971) shows that distributions of this quantity vary little with the flow Reynolds number for $K = 0$. Plots of $\overline{uv}/\overline{u^2}$ derived from the present measurements are given in figure 11. On the

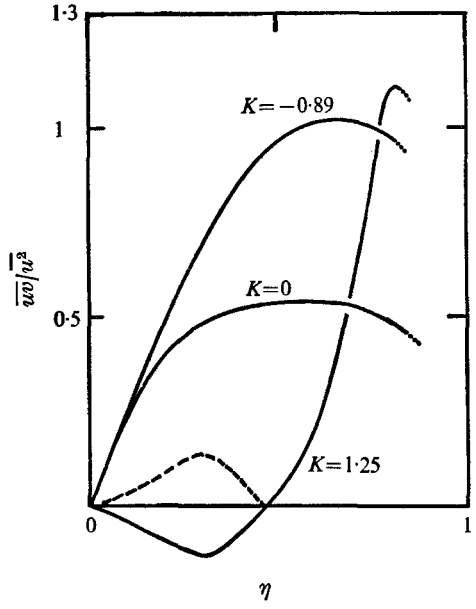

FIGURE 11. Measured distributions of the shear coefficient $\overline{uv}/\overline{u^2}$ for normal and distorted pipe flows. ---, $|\overline{uv}|/\overline{u^2}$.

basis of these results it is clear that the assumption of an invariant distribution of the shear coefficient is not reasonable, at least for distorted pipe flows. In fact some analytical studies of boundary layers have indicated that solutions of the energy equation are rather insensitive to the assumed a_1 distribution. The negative values of $\overline{uv}$ which occur away from the pipe centre-line for $K > 1$ are in themselves inconsistent with a distribution of the shear coefficient which is independent of K, as zero values of the shear stress away from the centre would unrealistically imply zero local values of the turbulence intensity and thus the dissipation. As with the mixing-length assumption the diffusion of turbulent energy must effectively be ignored at these positions, i.e. any assumption for the diffusion term in (18) must be constrained to give zero diffusion where $\overline{uv} = 0$ away from the pipe wall when the shear-coefficient assumption is made. It is of course possible to formulate new empirical forms of the shear-coefficient assumption which will overcome this difficulty but the derivation of empirical forms to satisfy a unique class of flows is not a productive exercise. The shear-coefficient assumption in its usual form thus appears to have no more validity than the mixing-length and eddy-viscosity assumptions for the pipe flows described here.

The available measurements permit a discussion of the turbulent energy balance with particular reference to the diffusion term. As described above, the turbulence intensity troughs found for positive K and the flattening of the intensity distribution found for negative K can be linked qualitatively with the production term of the turbulent energy equation, although direct linking of the shear stress with the local turbulence intensity does not seem to be valid. The approximate turbulent energy balance for $K = 1{\cdot}25$ shown in figure 12 was

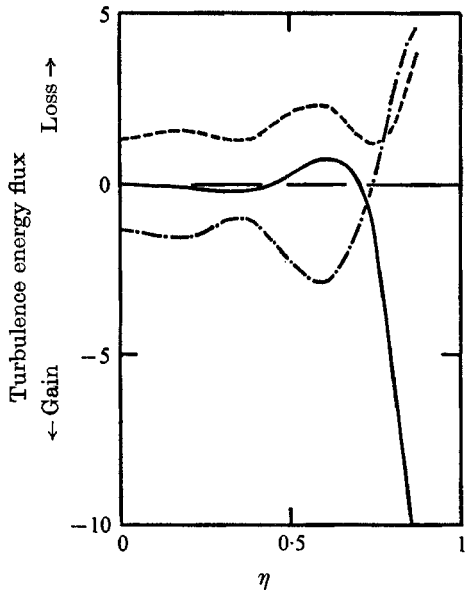

FIGURE 12. Turbulent energy balance for distorted pipe flow with $K = 1{\cdot}25$. ——, production, $(R/u_\tau^3)\,\overline{uv}\,\partial U/\partial r$; – – –, dissipation, $(R/u_\tau^3)\,\epsilon$; —·—, diffusion, $(R/u_\tau^3)\,r^{-1}\partial(\frac{1}{2}\overline{q^2v}r + \overline{pv}r)/\partial r$.

derived by making an assumption for the dissipation term, $\overline{uv}\,\partial U/\partial r$ being known and the diffusion term being derived from the difference of the other two terms. It was assumed that $\epsilon = (\overline{u^2})^{\frac{3}{2}}/l_\epsilon$, which is Townsend's (1961) expression with the assumption that $\overline{u^2}$ is everywhere the same fraction of the total turbulence intensity $\overline{q^2}$. Laufer's data indicate that l_ϵ can be assumed to be constant across most of the pipe but $l_\epsilon = O(R-r)$ in the wall region (where measurements were not possible in the present experiments). The value $l_\epsilon/R = 0{\cdot}27$ gave good agreement between the present energy balance for the pipe flow with $K = 0$ and Laufer's energy balance. For normal pipe flow Laufer's results show that the pressure and kinetic-energy components of the diffusion term either cancel each other out or are negligible except very near the wall and in the central region, $0 < \eta < 0{\cdot}4$ say, where the production term becomes small. However, figure 12 shows that the diffusion term is important over the complete width of the distorted flow with $K = 1{\cdot}25$ and for half of the pipe width, $0 < \eta < 0{\cdot}5$, the production term is negligible and the diffusion and dissipation terms are equal and opposite in sign. On the wall side of the mean velocity peak the dissipation and diffusion terms are almost equal but of the same sign: a phenomenon which does not occur in normal pipe flow but exists in the high-intensity regions of free shear flows. Examination of the shape of the diffusion-term distribution and comparison of it with the $(\overline{u^2})^{\frac{1}{2}}/u_\tau$ curve for $K = 1{\cdot}25$ in figure 9 indicate that a simple gradient diffusion assumption for the turbulent energy would not be valid, for example this would require zero values of the diffusion term at or near inflexion points in the $\overline{u^2}/u_\tau^2$ distribution. In addition the assumption of a bulk convection process (with $\frac{1}{2}\overline{q^2v} + \overline{pv} = \frac{1}{2}V\overline{q^2}$ and the bulk convection velocity $V(\eta)$ having

a similar distribution to that for normal pipe flow) is unlikely to predict the observed energy-term distributions. It is possible that a combined gradient diffusion and bulk convection process similar to that of Keffer (1965) is the most reasonable assumption as this could account for the appearance of the diffusion-term distribution as a gradient diffusion curve which has been displaced vertically. Alternatively bulk convection may indeed dominate the diffusion process but the controlling large eddies may have structures which are strongly dependent on the extra body forces applied to the flow, so that $V(\eta)$ is also a function of K.

No attempt has been made to analyse this approximate energy balance in a quantitative way as fuller and more accurate turbulence measurements are needed, including data for the wall region. The balance for a positive value of the body-force parameter K has been discussed as this produced the most interesting results; the flows with negative values of K suffered considerably less distortion. It should be noted that the objective of obtaining distorted velocity distributions in the pipe flows required the application of body forces which were rotational ($\text{curl}\,\mathbf{F} \neq 0$) as irrotational forces would merely have resulted in the production of balancing pressure fields. The use of dimensional analysis to derive modified 'log law' velocity distributions for the distorted flows (analogous to those for pipe flows with rough walls or suction) is not possible because of the rotational nature of $\mathbf{F}$.

6. Conclusions

Fully developed but severely distorted turbulent pipe flows have been produced by using electromagnetic body forces and the potential of this technique for gaining further insight into the mechanisms of turbulent flow has been demonstrated. The experiments have shown the inaccuracies of assumptions of mixing-length and eddy-viscosity type and they have permitted discussion of the terms in the turbulent energy equation and their simplification. In particular the importance of the diffusion term in the energy equation was demonstrated. An extensive investigation of this type of distorted flow for a wider range of distortion would provide quantitative information on the various turbulence assumptions and would produce, for example, quantitative values of the bulk convection and gradient diffusion contributions to the flow. The velocity profiles with inflexion points which were produced for laminar pipe flows would seem to be of interest in flow stability studies.

This investigation was originated by M. K. Bevir, who also carried out initial work on the design of the apparatus. The author thanks Professor J. A. Shercliff for his advice during the investigation and the Science Research Council for providing a grant.

REFERENCES

BRODKEY, R. S., NYCHAS, S. G., TANAKE, J. L. & WALLACE, J. M. 1973 Turbulent energy production, dissipation and transfer. *Phys. Fluids*, **16**, 2010–2011.

HALL, W. B. & JACKSON, J. D. 1969 Laminarization of a turbulent pipe flow by buoyancy forces. *A.S.M.E.–A.I.Ch.E. Heat Transfer Conf., Minneapolis, A.S.M.E. Paper*, 69-HT-55.

KEFFER, J. F. 1965 The uniform distortion of a turbulent wake. *J. Fluid Mech.* **22**, 135–159.

LAUFER, J. 1955 The structure of turbulence in a fully developed pipe flow. *N.A.C.A. Rep.* no. 1174.

LAWN, C. J. 1971 The determination of the rate of dissipation in turbulent pipe flow. *J. Fluid Mech.* **48**, 477–505.

SCHEELE, G. F. & GREENE, H. L. 1966 Laminar–turbulent transition for nonisothermal pipe flow. *A.I.Ch.E. J.* **12**, 737–740.

SCHLICHTING, H. 1968 *Boundary Layer Theory*. Pergamon.

SHERCLIFF, J. A. 1965 *A Textbook of Magnetohydrodynamics*. Pergamon.

TOWNSEND, A. A. 1961 Equilibrium layers and wall turbulence. *J. Fluid Mech.* **11**, 97–120.